Active Anionic Zero-Valent Palladium Catalysts: Characterization by Density Functional Calculations

Sebastian Kozuch,[a] Sason Shaik,*[a] Anny Jutand,[b] and Christian Amatore[b]

Abstract: This works uses DFT (B3LYP/LACVP*+//B3LYP/LACVP* level) to ascertain the existence of the tricoordinate, anionic zero-valent palladium complexes that were postulated as the active species in the catalytic cycles of Pd-catalyzed Heck and cross-coupling reactions. The variety of complexes studied (**1** and **2**), include $[Pd(PR_3)_2X]^-$ species, in which R = H, Me, vinyl, and phenyl, and X = Cl, Br, I, AcO, and TFA, as well as bidentate complexes, $[Pd\{Ph_2P(CH_2)_nPh_2P\}X]^-$, in which X = Cl, AcO and n = 3–6. The study shows that these complexes exist as distinct minima in the gas phase as well as in THF. In addition, it provides geometric features and Pd–X^- dissociation energies for all these complexes as well as some NMR and IR data, which show a clear distinction in these features between the tri- and dicoordinate Pd^0 species. An orbital interaction model and perturbation theory arguments account for the bonding mechanism *and rationalize all the trends in the stability of the Pd–X bond.* These trends include the effects of variation of X, R, and the length of the linker in the bidentate ligands.

Keywords: cross-coupling · density functional calculations · Heck reaction · ligand effects · palladium

Introduction

Palladium is a versatile catalyst of organic reactions, capable of formation of a variety of bonds (C–C, C–H, C–N, C–O, C–P, C–S, C–CO–C, etc.) by means of named reactions such as the Heck, Tsuji–Trost, Suzuki, Sonogashira, and cross-coupling reactions.[1] Part of the efficacy of palladium is its ability to cleave C–X (X = halide, AcO, etc.) bonds in its zero-valent state, by an oxidative addition that provides an organopalladium(II) complex, which is prone to react with nucleophiles. The newly formed organopalladium(II) complex continues the catalytic cycle that eventually leads to products and regenerates the palladium(0) complex. A textbook representation of such a catalytic cycle, for example, the cross-coupling reaction with hard nucleophiles is depicted in Scheme 1a, which shows that the active species is simple the 12-electron $[Pd^0L_2]$ complex.

Following a series of mechanistic investigations by two of us (A.J. and C.A.),[2–6] it has been shown that the actual catalytic cycle is the one depicted in Scheme 1b, whereby the active species in oxidative additions is a trivalent complex, for example, $[Pd^0L_2Cl]^-$, that is formed when the $[Pd^0L_2]$ species takes up a Cl^- ionic additive. Such an active species was proposed with a variety of additives, like Br^-,[3] I^-,[3] AcO^-,[7–9] and TFA^- (trifluoro acetate)[10] and so forth. While there is indirect evidence for the presence of this active species in the cycle, that is, NMR and kinetic-type evidence, the species itself has never been isolated and its characteristics remain obscured. This situation calls for the interplay of theory and experiment. The goal of the present paper is to address the existence of the putative active anionic Pd^0 species by computational means and answer the following questions: Does it really exist as a discrete entity? What are its geometric and spectral features? What is the strength of the bond between Pd and the additive anion X^-? What are the bonding characteristics of the Pd–X^- bond, and how does this vary with the nature of X^- and the identity of the other two ligands on the palladium center? As an application we have decided to explore the features of two types of complexes: complexes **1**, with two phosphine ligands, and $\mathbf{2}_n$, with the bidentate diphenylphosphine ligand held by a $(CH_2)_n$ chain (n = 3 -dppp-, n = 4 -dppb-, n = 5 -dpppe-, n = 6 -dpph-). Some of these complexes, for example, $\mathbf{1}_{Ph,X}$ (X = Cl, Br, I, AcO, TFA^-), were studied experimentally,[3,8–10] while others like $\mathbf{1}_{H,X}$ are simplified models designed to define the minimalist systems that mimic faith-

[a] S. Kozuch, S. Shaik
Department of Organic Chemistry and Lise Meitner–Minerva Center for Computational Quantum Chemistry
Givat Ram Campus, Jerusalem 91904 (Israel)
Fax: (+972) 265-84-680
E-mail: sason@yfaat.ch.huji.ac.il

[b] A. Jutand, C. Amatore
Ecole Normale Supérieure
Département de Chimie UMR CNRS-ENS-UPMC 8640
24 Rue Lhomond, 75231 Paris Cedex (France)

 © 2004 Wiley-VCH Verlag GmbH & Co. KGaA, Weinheim DOI: 10.1002/chem.200306056

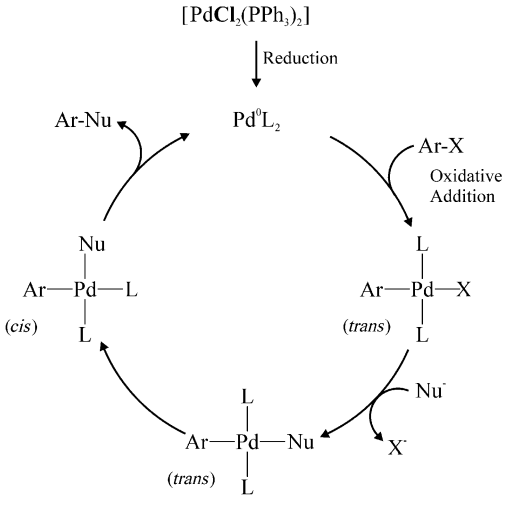

a) Textbook Mechanism

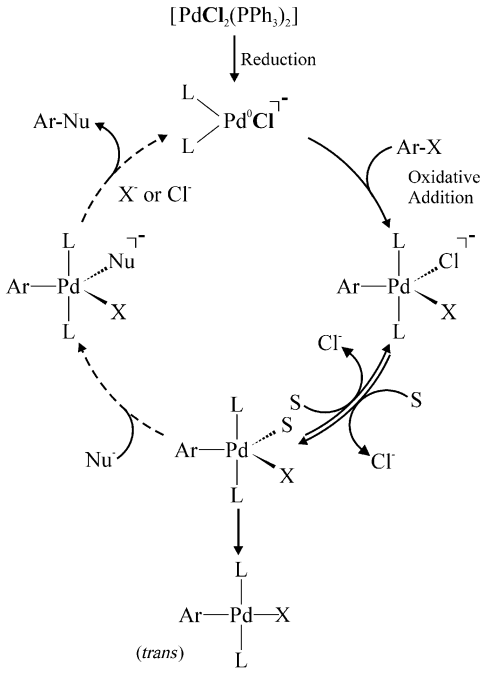

b) New Mechanism (S = solvent)

Scheme 1. a) The textbook cycle vis-à-vis. b) The Jutand–Amatore cycle.

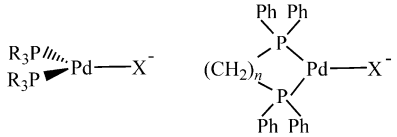

1 **2**

fully the experimental species. As we shall demonstrate the proposed active species exist as discrete entities in *both* the gas phase and in THF, and possess *finite* Pd–X^- bond energies that depend critically on the nature of the phosphine ligand and on the size of the chelating ring as well as on the identity of the X^- ion.

Computational Methods

Density functional theory (DFT) was used throughout the study with the hybrid density functional, B3LYP, which is considered by and large as a reliable quantum chemical method for large molecules, and for palladium complexes as well.[11] Since none of these complexes has ever been characterized experimentally it was necessary to benchmark the method and to ascertain that it leads to converged properties. In addition, since the PPh_3 ligands are quite large, we sought for smaller models that are still reliable. We therefore studied, for $[Pd(PR_3)_2X]^-$ (**1**) and $[Pd(R_2P(CH_2)_nPR_2)X]^-$ (**2**$_n$), the following matrix of basis sets and models schematized in Table 1.

The first variable in this matrix is the basis set, which varies from the double-zeta quality, LACVP[12,13] all the way to LACVP**$^{++}$. SCF convergence difficulties prohibited a routine use of triple-zeta basis sets in the LACVP series. The LACVP basis set, implemented in JAGUAR 4.2,[13] describes the Pd atom with an effective core potential and a double-zeta valence basis set, while the rest of the atoms are described by a 6-31G Pople basis set.[14] The LACVP* basis adds polarization functions on the P, Cl, and C atoms, while the LACVP$^+$ equips these atoms with diffuse functions. LACVP** adds polarization functions on the hydrogen atoms and so does LACVP^{++} with respect to diffuse functions. The designation LACVP*$^+$(aug) means that the LACVP*$^+$ basis set was augmented on the Pd atom by polarization functions (f with exponent 0.211) and diffuse ones (+ with exponent 0.057), the exponents of which were optimized in Gaussian 98[14] for $\mathbf{1}_{H,Cl}$.

This benchmark study provided us a small library of results, which allowed us to select a basis set and a model that can serve in the future for routine study of these complexes and their reactivity. It was thus found that B3LYP/LACVP* geometries, with single-point B3LYP/LACVP*$^+$ energies, gave almost the same results as the B3LYP/LACVP**$^{++}$ basis set or better ones (less than 1 kcal mol^{-1} for Pd–Cl and Pd–P dissociation energies), for all the model systems. Basis set superposition errors for the LACVP*$^+$ basis set lowered the bond energies by small amounts (0.6, 1.2, 0.8 kcal mol^{-1} for L PH_3, X = I, Br, Cl, respectively). Furthermore, a single-point calculation with the LACVP*$^+$(aug) basis set showed a small increase of the bond energies, with differences that ranged from 0.1 to 0.8 kcal mol^{-1} (from X = I to X = Cl), relative to the LACVP*$^+$ basis set. Thus, the B3LYP/LACVP*$^+$ energies were deemed sufficiently accurate for our purposes. This level, in the common notation B3LYP/LACVP*$^+$// B3LYP/LACVP* and in shorthand LACVP*$^+$//LACVP*, was used routinely for the other complexes. In addition, for the series of halide complexes **1**, X = Cl, Br, and I, we tried a variety of other basis sets on the halides; a double-zeta all-electron DZVP basis set, a 6-311G* Pople basis set, and effective core potentials plus matching basis sets, LANL2DZdp, the Stuttgart effective core potential (ECP)[15] with the recommended basis sets, and the aug-cc-pVQZ (SDB ECP for Br and I) basis sets as recommended and adapted by Martin.[16] The following sections discuss only those levels deemed reliable.

Jaguar 4.2 was used for geometry optimization.[13] For single-point energies at higher basis sets, Jaguar 4.2 was used in all the calculations that included LACVP family[13] of basis sets. For the other basis sets, the energies were calculated with Gaussian 98. Frequency calculations were done with Gaussian 98, which has a more accurate frequency calculation routine. All stable geometries were confirmed by having only real frequencies. Solvent calculation, including geometry optimization, was carried out with JAGUAR[13,17] by using the parameters of the solvent THF (molecular weight = 72.1, dielectric constant = 7.52, density = 0.886), which was employed in the experiment.[9] An alternative modeling of the species in a solvent was done by embedding the tricoordinate complex in a cluster of six THF molecules, while surrounding the cluster with a continuum that had the THF parameters. NMR calculations were carried out in Gaussian 98 with the DFT/GIAO method at the B3LYP/LACV3P**$^{++}$ level.[18] All the charges were calculated by use of the Mullikan charge analysis.

 © 2004 Wiley-VCH Verlag GmbH & Co. KGaA, Weinheim

Table 1. Basis sets and ligands studied for $\mathbf{1}_{R,X}$ and $\mathbf{2}_n$ ($n=3$–6).[a]

R, X	Basis set for all atoms		Basis set for Pd[c,d]	Basis set for X[e]					
	LACVP series[b]	LACVP*+	LACVP*+ (aug)	DZVP (DFT orbital)	LANL2DZdp ECP[c]	6 311G*	Stuttgart RLC ECP[c]	aug-cc-pVQZ	SDB-aug-cc-pVQZ[c]
H, Cl	**1**	**1**	**1**						
Me, Cl	**1**	**1**							
V, Cl		**1**							
Ph, Cl	**1**	**1**, $\mathbf{2}_{4,5,6}$	**1**	**1**	**1**	**1**	**1**	**1**	
Ph, Br		**1**	**1**	**1**	**1**	**1**	**1**	**1**	**1**
Ph, I		**1**	**1**	**1**	**1**	**1**	**1**		**1**
Ph, AcO		**1**, $\mathbf{2}_{3,5}$							
Ph, TFA^-		**1**							

[a] The identity of the species studied by a given basis set, is indicated in entries as **1** or $\mathbf{2}_n$. [b] Defined as follows: LACVP, LACVP*, LACVP**, LACVP+, LACVP++, LACVP*+, LACVP**+, LACVP*++, LACVP**++. ECP for Pd, Br, I. [c] ECP basis set. [d] LACVP*+ for all other atoms, except for Br and I, for which LANL2DZdp was used. [e] LACVP*+ for all other atoms.

Results

Choice of the model for 1—comparison of the $\mathbf{1}_{Ph,Cl}$, $\mathbf{1}_{Me,Cl}$, $\mathbf{1}_{H,Cl}$ and $\mathbf{1}_{V,Cl}$ complexes: Frequency calculations of the optimized structures of the four complexes revealed that with the exception of $\mathbf{1}_{Me,Cl}$, which possessed an imaginary frequency, all the others were stable minima. The imaginary frequency of $\mathbf{1}_{Me,Cl}$, corresponded to the out-of-plane bending of the chloride, and upon a tighter LACVP* optimization the methyl complex dissociated to the dicoordinate neutral $[Pd(PMe_3)_2]$ complex, with Cl^- attached to it by "hydrogen bonds" to the C–H bonds of the methyl groups. The general shapes of the LACVP* optimized structures of all the stable species are depicted in Figure 1. Consequently PMe_3 appears to be not only a poor but also a wrong model for PPh_3.

Consideration of the Pd–Cl dissociation energies (D), at the LACVP*+/LACVP* level, shows that $\mathbf{1}_{H,Cl}$ has smaller values than those calculated for the experimental model system, $\mathbf{1}_{Ph,Cl}$ ($D_{Pd-Cl}=8.06$ vs 12.02 kcal mol^{-1}). As such, PH_3 is not a perfect model for PPh_3. Thus, $\mathbf{1}_{Me,Cl}$ is a poor model, while $\mathbf{1}_{H,Cl}$ an unsatisfactory one (but cheap for theoretical calculations) for the experimental system $\mathbf{1}_{Ph,Cl}$. By contrast to these complexes, the one with the vinyl groups, $\mathbf{1}_{V,Cl}$, was found to possess bond dissociation energies on a par with the experimental species $\mathbf{1}_{Ph,Cl}$ ($D_{Pd-Cl}=11.39$ vs 12.02 kcal mol^{-1}). Moreover, inspection of the geometric details in Figure 1 (see also Table 3 later) shows that $\mathbf{1}_{V,Cl}$ and $\mathbf{1}_{Ph,Cl}$ have similar Pd–Cl bond lengths. An interesting structural feature that is common to the two complexes are the two hydrogen atoms of the Ph or V substituents that point towards the chloride ion and may clamp it by electrostatic attraction, thereby stabilizing the Pd–Cl^- bond.

In conclusion, therefore, the stability of the complexes of the type $\mathbf{1}_{R,Cl}$ exhibits a strong dependence on R, the substituent of the phosphine ligand; methyl and hydrogen result in unstable or weakly bound complexes, whereas vinyl and phenyl give stable complexes with more robust bonding energies. More on the origins of this substituent effect is elaborated in the discussion of the Pd–Cl^- bonding.

Comparison of $\mathbf{1}_{Ph,X}$ (X = Cl, Br, I, AcO, TFA): The general structural features of these complexes are depicted in Figure 2, at the B3LYP/LACVP* level, while Tables 2 and 3 provide bond-energy data. The bond energies determined by use of single-point LACVP*+ calculations gave, initially, an irregular trend in the Pd–X^- bond dissociation, with a peak for the Pd–Br^- bond. Since this basis set lacks, in fact,

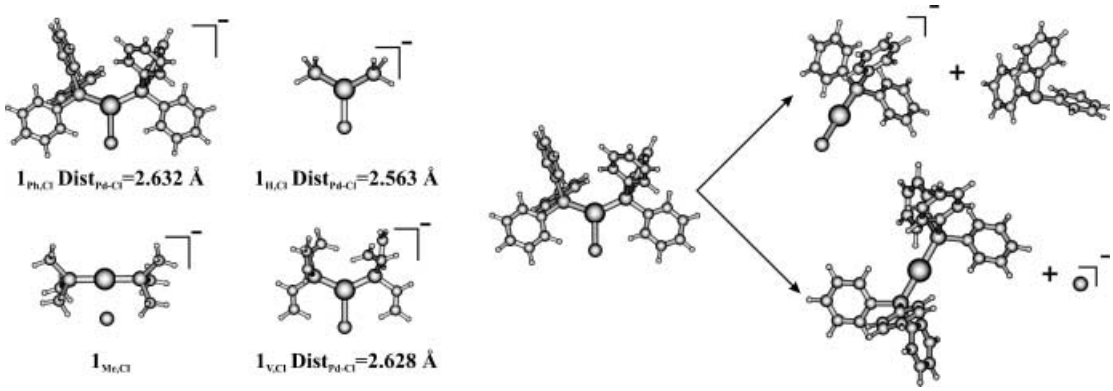

Figure 1. Optimized Structures of $\mathbf{1}_{R,Cl}$. Pd–P and Pd–Cl dissociation. Pd–Cl bond lengths ($Dist_{Pd-Cl}$) are indicated. The processes used to study the dissociation energies are shown on the right hand side (disociated fragments were calculated at infinite distance).

© 2004 Wiley-VCH Verlag GmbH & Co. KGaA, Weinheim

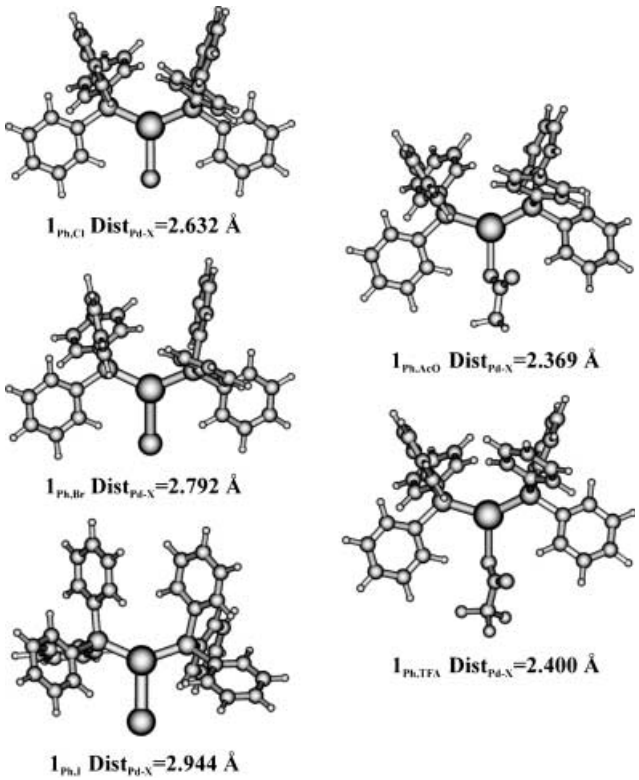

Figure 2. Optimized geometries of $\mathbf{1}_{Ph,X}$. The Pd–X bond lengths are indicated as $Dist_{Pd-X}$.

Table 2. Dissociation energies [kcal mol^{-1}] of the Pd–X$^-$ bonds for $\mathbf{1}_{Ph,X}$ in different basis sets.[a]

	LACVP*$^+$	LANL2DZdp ECP	Stuttgart RLC ECP	aug-cc-pVQZ	SDB-aug-cc-pVQZ
Cl	12.02		11.38	13.19	
Br	22.46	9.19	7.98	10.18	9.93
I	15.60	7.89	7.04		7.45

[a] Geometry in LACVP*.

the polarization and diffuse functions for Br$^-$ and I$^-$, we tried a variety of basis sets and ECPs in order to elucidate the correct trend in the bond energy. Table 2 shows the converged results by using Stuttgart RLC ECP, LACVP*$^+$, and aug-cc-PVQZ basis sets for Cl$^-$; the Stuttgart RLC ECP, LACVP*$^+$, LANL2DZdp ECP, aug-cc-PVQZ, and SDB-aug-cc-PVQZ (ECP) basis sets for Br$^-$; and Stuttgart RLC ECP, LACVP*$^+$, LANL2DZdp ECP, and SDB-aug-cc-PVQZ (ECP) basis sets for I$^-$. All these basis sets for the halides contain polarizations and diffuse functions, which are crucial at the dissociation limit at which the halide departs as an anion. Inspection of Table 2 shows that the D_{Pd-Cl^-} datum, obtained with LACVP*$^+$, is in accord with the large basis set calculation. The same applies to D_{Pd-AcO^-} and to any first-row anionic ligand. For the second-row anions, a bigger basis set (SDB-aug-cc-PVQZ) is necessary. A cheaper alternative is the LANL2DZdp ECP/basis set, which includes polarization and diffuse functions on the second-row anions. In conclusion, the results of the bigger and the balanced basis sets in Tables 2 and 3 establish a consistent trend: $D_{Pd-Cl^-} > D_{Pd-AcO^-} \geq D_{Pd-Br^-} > D_{Pd-I^-}$, and $D_{Pd-TFA^-} < D_{Pd-AcO^-}$.

Unlike the bond dissociation energies that require diffuse and polarization functions on the X ligand, the geometries of the $\mathbf{1}_{Ph,X}$ complexes were found to be less sensitive to the quality of the basis set beyond LACVP*. Table 3 shows the LACVP* optimized geometries, which exhibit a regular and expected tendency in the Pd–X bond length (X = Cl, Br, I, AcO, TFA). It grows as the atomic number of the ligand atom increases, going from 2.369 Å for the oxygen atom of the acetate ion (dissociation energy 10.51 kcal mol^{-1}) to 2.944 Å for the I$^-$ ion. Comparisons of the data for X = Cl$^-$ versus X = AcO$^-$ and X = TFA versus X = AcO$^-$ indicate that as the X$^-$ ion becomes a better electron donor, the Pd–X$^-$ bond gets stronger.

Are the complexes $\mathbf{1}_{R,Cl}$ (R = Ph, V) stable also in a solvent? Since all the experiments were done in THF, it was deemed necessary to test its stability in a solvent. The parameters of THF (see Computational Methods section) were used in the continuum solvent model of JAGUAR[13] to check the stability of $\mathbf{1}_{Ph,Cl}$ and $\mathbf{1}_{V,Cl}$. Alternatively, in the case of the $\mathbf{1}_{H,Cl}$ complex, we embedded the complex in a cluster of six THF molecules and then optimized the structure in a dielectric medium corresponding to continuum THF. The results, with or without the discrete THF cluster were virtually identical; this clearly shows that the species are real minima in a solvent. The results are shown in Table 4. As might be expected, the two complexes exhibit some elongation of the Pd–Cl distance with a concomitant increase of the anionic charge on the chloride atom. The solvent could also decrease the

Table 3. Pd–X$^-$ bond dissociation energy, geometric parameters, and charges for the tricoordinate Pd^0 complexes $\mathbf{1}_{Ph,X}$.

	D_{Pd-X}[a] [kcal mol^{-1}]	Distances [Å] Pd–X	Pd–P1	Pd–P2	P-Pd-P	Angles [°] X-Pd-P1	X-Pd-P2	Charges[a] X	Pd	$(PR_3)_2$
$\mathbf{1}_{H,Cl}$	8.06	2.563	2.288	2.291	124.1	119.5	116.3	−0.61	−0.15	−0.24
$\mathbf{1}_{V,Cl}$	11.39	2.628	2.307	2.306	130.4	114.8	114.8	−0.68	−0.24	−0.08
$\mathbf{1}_{Ph,Cl}$	12.02	2.632	2.321	2.322	132.9	113.9	113.2	−0.66	−0.33	−0.01
	(13.19)[b]							(−0.69)	(−0.29)	(−0.02)
$\mathbf{1}_{Ph,Br}$	9.93[b]	2.792	2.317	2.320	130.8	114.7	114.5	−0.71	−0.22	−0.07
$\mathbf{1}_{Ph,I}$	7.45[b]	2.944	2.317	2.322	136.5	113.8	109.3	−0.66	−0.26	−0.08
$\mathbf{1}_{Ph,AcO}$	10.51	2.369	2.299	2.312	135.9	106.7	117.4	−0.73	−0.20	−0.07
$\mathbf{1}_{Ph,TFA}$	4.82	2.400	2.312	2.324	137.6	118.6	103.6	−0.79	−0.23	0.02

[a] LACVP*$^+$//LACVP* data, unless noted otherwise. [b] LACVP*$^+$(aug-cc-pVQZ)//LACVP* for Cl; SDB-aug-cc-pVQZ(LACVP*$^+$) for Br and I. The basis set on the non-halogen is LACVP*$^+$ (see notation in the parentheses).

 © 2004 Wiley-VCH Verlag GmbH & Co. KGaA, Weinheim

Table 4. Optimized geometric parameters and charges of $\mathbf{1}_{Ph,Cl}$ and $\mathbf{1}_{V,Cl}$ in the gas-phase and in THF (basis set LACVP*+//LACVP*).

		Distances [Å]			Angles [°]			Charges		
		Pd–Cl	Pd–P1	Pd–P2	P-Pd-P	Cl-Pd-P1	Cl-Pd-P2	Cl	Pd	P-Ligand
$\mathbf{1}_{Ph,Cl}$	gas phase	2.632	2.321	2.322	132.9	113.9	113.2	−0.66	−0.33	−0.01
	THF	2.790	2.336	2.351	140.2	112.9	106.8	−0.87	−0.22	0.09
$\mathbf{1}_{V,Cl}$	gas phase	2.628	2.306	2.307	130.4	114.8	114.8	−0.68	−0.24	−0.08
	THF	2.770	2.322	2.321	134.7	112.4	112.9	−0.86	−0.25	0.11
$\mathbf{1}_{H,Cl}$	gas phase	2.563	2.288	2.291	124.1	119.5	116.3	−0.61	−0.15	−0.24
	THF[a]	2.718	2.304	2.321	122.9	110.2	126.8	−0.82	−0.06	−0.12
		(2.706)	(2.306)	(2.314)	(129.8)	(114.4)	(115.8)	(−0.75)	(0.14)	(−0.23)

[a] Datum in parenthesis corresponds to calculation with a cluster of THF embedded in a continuum THF.

$Pd–Cl^-$ bond dissociation energy, but this effect is not so straightforward to compute.

The effect of ring size of the bidentate ligand in the 2_n complexes: 1,4-Bis(diphenylphosphino)butane (dppb) is a classical bidentate ligand that has been used extensively to form complexes with palladium.[3–9] In this respect, one wonders what is the effect of using a bidentate ligand versus two PPh_3 ligands in $\mathbf{1}_{Ph,X}$, and what role is played by the chain length in the bidentate ligand. Figure 3 shows the optimized

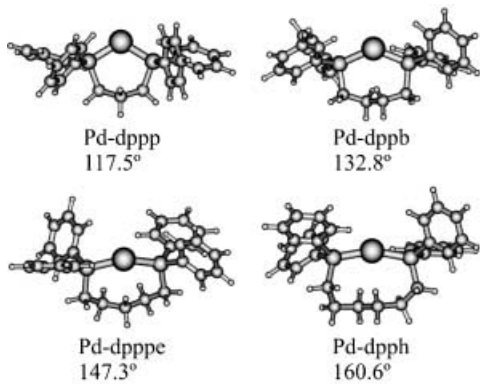

Figure 3. Optimized structures for Pd–dpph, Pd–dpppe, Pd–dppb and Pd–dppp fragments with their P-Pd-P angle.

structures of the bidentate complexes, while the Table 5 gives the $Pd–Cl^-$ bond dissociation energies of these species

Table 5. $Pd–X^-$ dissociation energies and P-Pd-P Angles for complexes with bidentate phosphine ligands.

	P-Pd-P angle; radians (degrees)[a]		D_{Pd-Cl} [D_{Pd-AcO}] [kcal mol^{-1}][a]
	dicoordinate complex	tricoordinate complex with Cl [AcO]	
$Pd(PPh_3)_2$	1.00 (179.3)	0.73 (132.9) [0.75 (135.6)]	12.02
Pd–dpph	0.89 (160.6)	0.75 (136.8)	11.29
Pd–dpppe	0.82 (147.3)	0.74 (132.4) [0.75 (135.1)]	14.17 [13.33]
Pd–dppb	0.74 (132.8)	0.62 (113.8)	16.91
Pd–dppp	0.65 (117.5)	[0.60 (108.3)]	[18.76]

[a] Geometries with LACVP*, while energies with LACVP*+. Results for X = OAc^- are in square brackets.

vis-à-vis the $\mathbf{1}_{Ph,Cl}$ complex (or Pd-AcO^- against $\mathbf{1}_{Ph,AcO}$). It is seen that the dppb ligand in $\mathbf{2}_4$ increases the bond dissociation energy by more than 40% relative to the $\mathbf{1}_{Ph,Cl}$ complex. However as the chain of the bidentate ligand lengthens, the bond energy converges virtually to the value for the $\mathbf{1}_{Ph,Cl}$ complex.

Table 5 lists the P-Pd-P angles in the di- and tricoordinate complexes, as well as the corresponding Pd-X^- (X = Cl, AcO) bond energies. Figure 4 shows a plot of the $Pd–Cl^-$

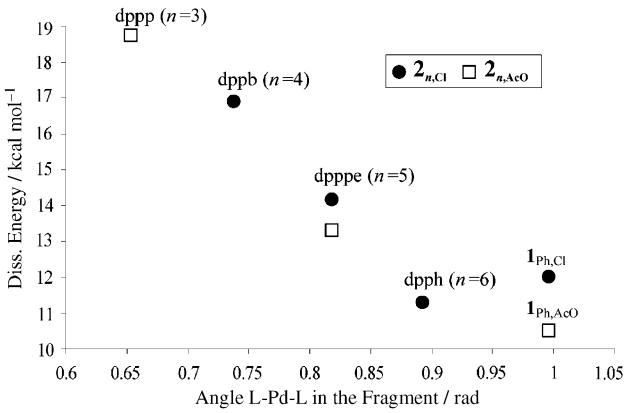

Figure 4. Pd–Cl (heavy circles) and Pd–OAc (squares) bond dissociation energies versus P-Pd-P angles in the dicoordinated complexes.

and $Pd–AcO^-$ dissociation energies versus the P-Pd-P angle (expressed in radians) of the [PdL_2] $\mathbf{2}_n$ complexes. The bond energies are seen to correlate with the angles, the smaller the angle the larger the bond energy. The bond energy increases as the angle in the dicoordinate complex decreases. Since the angle in the {$Pd(Ph_3P)_2$} dissociation fragment of $\mathbf{1}_{Ph,Cl}$ is virtually linear (1 rad in Table 5), the behavior of the bidentate complex must be rooted in the inability of the dissociated fragment to relax its P-Pd-P angle. The same is true for the two data points for the acetate complexes (squares in Figure 4). This will be further addressed in the Discussion section.

Some spectral features of $\mathbf{1}_{Ph,Cl}$ and $\mathbf{2}_n$: The calculations show that the harmonic IR frequency of the $Pd–Cl^-$ bond in the experimental system $\mathbf{1}_{Ph,Cl}$ and its best model $\mathbf{1}_{V,Cl}$ are 171–173 cm^{-1}. A similar value of 173 was found for the Pd–

© 2004 Wiley-VCH Verlag GmbH & Co. KGaA, Weinheim

Table 6. ^{31}P NMR chemical shifts.[a]

Molecule	δ [ppm]	Molecule	δ [ppm]
$\mathbf{1}_{\mathbf{Ph,Cl}}$	46.3	$\mathbf{1}_{\mathbf{V,Cl}}$	60.1
$\mathbf{1}_{\mathbf{Ph}}$	23.5	$\mathbf{1}_{\mathbf{V}}$	37.3

[a] DFT-GIAO//B3LYP/LACV3P**++. δ (H_3PO_4) = 241.7 ppm is used as reference (calculated in the same basis set). $\delta = \sigma(\mathbf{1}_{\mathbf{R,X}}) - \sigma(H_3PO_4)$. An averaged chemical shift for the two ^{31}P values that derive from the slightly different environment of the two phosphorus ligands in the calculations. Experimental values are given in reference [19].

AcO^- bond. Table 6 shows NMR ^{31}P chemical shift values calculated for $\mathbf{1}_{\mathbf{Ph,Cl}}$, $\mathbf{1}_{\mathbf{Ph}}$, $\mathbf{1}_{\mathbf{V,Cl}}$, and $\mathbf{1}_{\mathbf{V}}$.

The difference between the chemical shifts for the tri- and dicoordinate complexes is larger than the experimentally observed difference. This indicates that the complexes in solution have longer Pd–Cl bonds and wider P-Pd-P angles compared with the gas-phase situation. As such, theory shows that ^{31}P NMR chemical shift can be diagnostic of the uptake of an anion by the dicoordinate Pd^0 complex.[19]

Discussion

Our calculations show that the anionic tricoordinate Pd^0 complexes, postulated previously[3–10] based on kinetic and NMR studies, are indeed genuine minima with finite bond energies between the palladium and the anionic additive. The geometric and spectral features derived here may be helpful for future experimental characterization of these species. What we would like to do in this section is to propose a bonding model that accounts in a coherent manner for the findings of this study. Figure 5 shows the Kohn–Sham orbitals for $\mathbf{1}_{\mathbf{Ph,Cl}}$. It is seen that these orbitals constitute a complete set of bonding and antibonding orbitals with respect to the Pd–Cl linkage, and since the orbitals are all filled, the origins of the Pd–Cl bonding is not apparent. However, a closer look into the wave functions of these orbitals reveals a significant participation of the 5p orbitals of palladium in bonding; this might provide a reason for the finite Pd–Cl^- bond energy.

To understand the origins of Pd–X^- bonding, we use a fragment MO interaction diagram, in the style of the Hoffmann school.[20,21] We dissect the $\mathbf{1}_{\mathbf{Ph,Cl}}$ complex into the two fragments, $Pd(PPh_3)_2$ and Cl^-, and by mixing the fragment orbitals we seek a bonding mechanism. This interaction diagram is shown in Figure 6. Figure 6a shows a Walsh diagram[22] for the valence-shell MOs of a $[PdL_2]$ d^{10} complex in two geometries, one bent and one linear. It is seen that the bent complex has four low-lying occupied d orbitals ($1a_1$, $1b_1$, a_2, and $2a_1$ in C_{2v} notation) and one filled orbital of b_2 symmetry that is higher lying due to the antibonding interaction with the ligand orbitals. As the P-Pd-P angle opens up, the antibonding interaction is turned off and the b_2 orbital joins the other low-lying d orbitals (symmetry labels with respect to $D_{\infty h}$ are σ_g^+, π_g, δ_g). Thus, the d^{10} PdL_2 fragment prefers a linear structure. However, to bind an additional ligand, the fragment has to bend. One of the reasons being

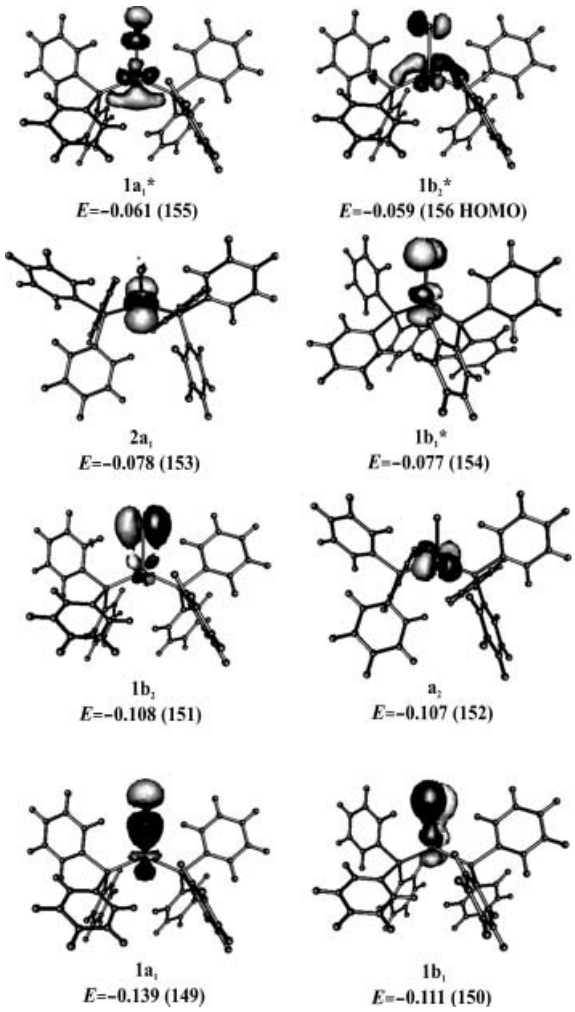

Figure 5. A few highest occupied orbitals of $\mathbf{1}_{\mathbf{Ph,Cl}}$, and their bonding features. We show also symmetry labels in C_{2v}, in keeping with the labels appearing in Figure 6b.

the $3a_1$ orbital, which becomes weakly bonding in the bent structure and, hence, is lowered in energy. This will enable the bent structure to mix strongly with another fragment that has an occupied orbital of the same symmetry, for example, Cl^-.

Figure 6b shows the interaction diagram for the bent PdL_2 fragment with the filled 3p orbitals of Cl^-. In the C_{2v} group, the 3p(Cl^-) orbitals transform as a_1, b_2, and b_1 symmetries, and will therefore have a symmetry match with the filled d orbitals of the PdL_2 fragment. Were they by themselves, these orbital interactions would have lead to a net antibonding character of the Pd–Cl^- bond. However, here the vacant 5p orbitals of Pd come to the rescue, and by mixing with the antibonding combinations ($1a_1$*, $1b_1$*, and $1b_2$*) from above they cause the last-mentioned orbitals to lower their energy. In the event that this 5p mixing is sufficiently strong, then there will be a net bonding interaction of the two fragments, and the Pd–Cl^- bond will have finite dissociation energy. The imprints of these mixings are seen in the total charge on the Cl^- and other anionic fragments in Table 3; the charge is significantly smaller than unity, indicating a significant charge transfer from the anionic ligand towards the

 © 2004 Wiley-VCH Verlag GmbH & Co. KGaA, Weinheim

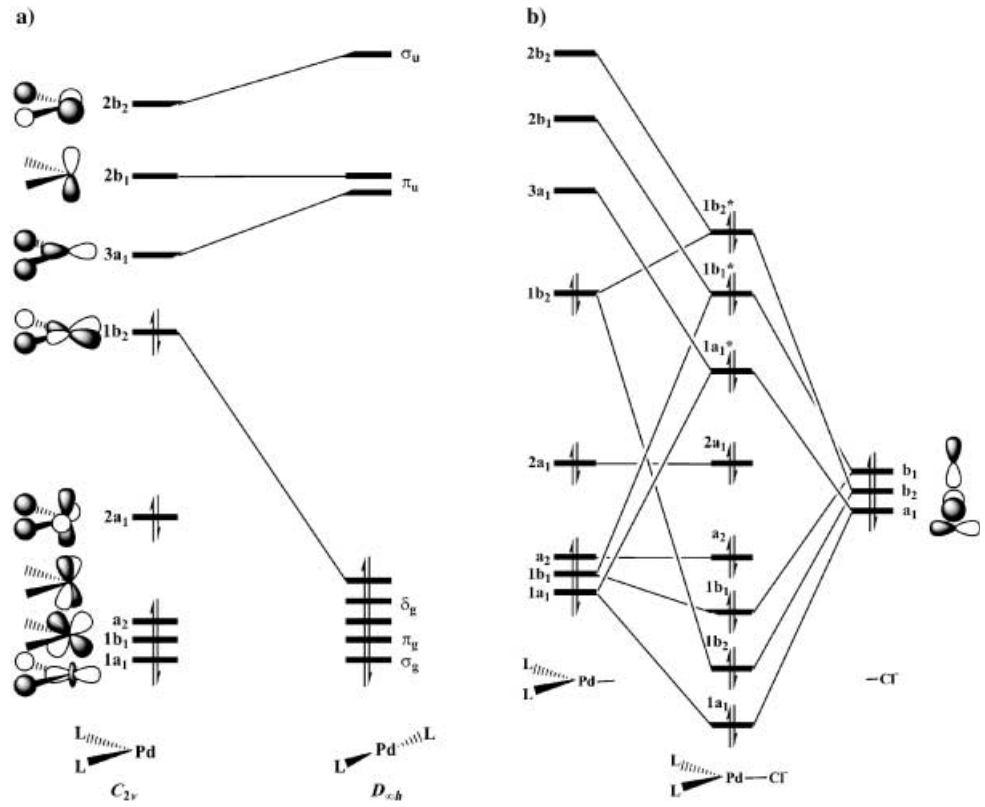

Figure 6. a) A Walsh diagram for PdL_2. b) An MO interaction diagram for PdL_2Cl^-. The frontier orbitals of the tricoordinate complex are generated from mixing of those of PdL_2 and Cl^-.

PdL_2 fragment. The stabilization energy (*SE*) due to this secondary mixing of the vacant 5p-type orbitals of Pd into antibonding combinations ($1a_1$*, $1b_1$*, and $1b_2$*) follows from perturbation theory and is given in Equation (1):

$$SE\,(5p\text{-}\phi^*) = \langle 5p|H|\phi^*\rangle^2/[\varepsilon_{\phi^*} - \varepsilon_{5p}] = \beta^2_{5p-\phi^*}/\Delta\varepsilon$$
$$\phi^* = 1a_1^*,\ 1b_1^*,\ \text{and}\ 1b_2^* \qquad (1)$$

Here, the first term is the matrix element between the interacting orbitals and the second term is their energy gap. The lower the 5p orbitals ($3a_1$, $2b_1$, and $2b_2$) of Pd, the stronger would their mixing be into the antibonding $1a_1$*, $1b_1$*, and $1b_2$* combinations, and the more significant the charge transfer would be. The simplest factor that affects the levels of these 5p orbitals is the electronegativity of the ligands (L) that are attached to Pd. The more electronegative these ligands are, the lower the 5p orbitals and the stronger is the mixing into the $1a_1$*, $1b_1$*, and $1b_2$* combinations. Especially important is the effect of electronegativity on the 5p($3a_1$) orbital on PdL_2. This orbital is weakly bonding with respect to the Pd–L linkages, and will be strongly affected by the electronegativity of L. Similarly, the 5p($2b_2$) orbital that is antibonding with respect to the Pd–L linkages, will also be lowered as the ligands become more electronegative. Finally, the 5p($2b_1$) orbital of PdL_2, will be affected in a similar fashion but to a lesser extent, since it is located only on Pd without contribution from the ligand.

Figure 6b and Equation (1) lead therefore to a few clear conclusions:

1) The Pd–Cl^- bond energy should increase as the other ligands on Pd become more electronegative.
2) For a variable anion additive, the Pd–X^- bond energy will be modulated by the donor ability of the X^- ion, such that in a series of anions from the same row, the better donor will possess the largest bond energy.
3) Since the free PdL_2 relaxes by going to a linear structure, any angular constraints that prevent this relaxation will increase the Pd-X^- dissociation energy.

The computational data appear to be in accord with these conclusions. Thus, the PMe_3 ligand is not an electron withdrawing species, and hence the Pd–Cl^- bond energy is negative. The PH_3 ligand, which is slightly more electronegative, has a positive, but small, bond energy. By contrast, PPh_3 and PV_3 have sp^2 carbon atoms, which withdraw electrons from the phosphorus ligand and make it more electronegative. Hence, it was with these ligands that we observed a more significant Pd–Cl^- bond energy. The acetate ligand is a lesser electron donor than Cl^-, and hence it participates less in mixing with the empty orbitals of PdL_2, and consequently the Pd–AcO^- bond is slightly weaker than the Pd–Cl^- bond. Similarly, the solvent stabilizes the Cl^- orbitals, lowers them in energy, and hence weakens the interactions with the empty orbitals of the Pd, leading to weakened Pd–Cl^- bond. The larger halides, Br^- and I^-, are better electron donors

© 2004 Wiley-VCH Verlag GmbH & Co. KGaA, Weinheim

than Cl^-, but nevertheless the bonds to Pd are weaker. This is a common trend that originates in the matrix element factor [Eq. (1)] that gets smaller in the higher row atoms. However, in solution the smaller the halide the greater is its stabilization by the solvent, and, hence, the solvent will apply a leveling effect and may even reverse the ordering, making the Pd–I^- bond the stronger in the series. Another interesting comparison is between the Pd–AcO^- and Pd–TFA^- bonds. Due to the high electronegativity of the fluorine substituents of TFA^-, the π(O) orbitals of the oxygen atom that are involved in the bonding with the vacant 5p orbitals on Pd are lowered relative to the situation in AcO^-, and the ϕ^*-5p mixing in Equation (1) decreases, and so does the bonding energy. The result is a Pd–TFA^- bond that is half as strong as Pd–AcO^-. Finally, the smallest bidentate ligand dppb investigated in Pd–Cl^- complexes cannot relax its P-Pd-P angle upon dissociation, and hence the Pd–Cl^- bond energy is quite large (17 kcal mol^{-1} in Table 5). However, as the $(CH_2)_n$ chain of the bidentate ligand gets longer, the PdL_2 fragment can increasingly relax its angle, and the bond dissociation energy converges to a value slightly lower than that of the complex $\mathbf{1}_{\mathbf{Ph,Cl}}$. The reason for the slightly lower value is that the bidentate ligands possess only two phenyl substituents on each phosphorus center in comparison with $\mathbf{1}_{\mathbf{Ph,Cl}}$, and since methyl substituents weaken the Pd–Cl^- bond energy, this bond is slightly weaker in the bidentate complexes with the large rings, in which the fragment can relax its P-Pd-P angle.

It is important to point out that the simple perturbational model of orbital interactions does not take into account other factors such as noncovalent interactions. As we pointed out in the Results section, in $[Pd(PPh_3)_2Cl]^-$ and $[Pd(PV_3)_2Cl]^-$, the C–H bonds of the organic substituent on the phosphorus atom are oriented towards the Cl^- ion. Since the H atoms are slightly positively charged, the C–H bonds clamp the anion by electrostatic interactions, which contribute to the bond energy. Nevertheless, the simple orbital model works well and lends itself to making clear predictions of trends in these complexes.

Conclusion

In this work we have investigated theoretically (DFT in B3LYP/LACVP*$^+$//LACVP*, as most commonly used level) the putative existence of tricoordinate palladium anionic complexes that are postulated as starting points for catalytic cycles by Amatore and Jutand.[5,6] The variety of complexes studied (**1** and **2**), include $[Pd(PR_3)_2X]^-$ species, whereby R = H, Me, vinyl, and phenyl, and X = Cl, Br, I, AcO and TFA, as well as bidentate complexes, $[Pd\{Ph_2P(CH_2)_nPh_2P)\}X]^-$, whereby X = Cl, AcO and n = 3–6. The study shows that these complexes exist as distinct minima in the gas phase as well as in THF. In addition, the work provides geometric features and Pd–X^- dissociation energies for all these complexes and some NMR and IR frequency data, which show a clear distinction compared with these features in the dicoordinate Pd^0 species.

An orbital interaction model [Figure 6b, Eq. (1)] accounts for the bonding mechanism and rationalizes the trends in the stability of the Pd–X bond. The anionic ligands that gave a better interaction with the empty 5p-type orbitals of the palladium also gave a more significant dissociation energy. Thus the tendency is $D_{Pd-Cl^-} > D_{Pd-AcO^-} \geq D_{Pd-Br^-} > D_{Pd-I^-}$. As we noted, in solution there may be a leveling off or even reversal of this trend.

The interaction diagram rationalizes also the effect of R, the substituent on the phosphorus ligand. Phenyl and vinyl apply an electron-withdrawing effect that lowers the antibonding orbitals of Pd (Figure 6b) and thereby enhance the interaction with the filled p orbitals of the anionic ligand. By contrast, when R = Me, the substituent is electron releasing and, hence, the antibonding orbitals of the $Pd(Me_3P)_2$ moiety of the neutral ligand are too high to interact efficiently with the orbitals of the anionic ligand, leading to a dissociative $[Pd(Me_3P)_2X]^-$ complex. The case of R = H is an intermediate one.

The bidentate ligands, $Ph_2P(CH_2)_nPh_2P$, with short linkers between the phosphorus centers were shown to lead to the largest Pd–X^- dissociation energies. However, as the linker gets gradually longer, the bond energy converges to values slightly lower than that of the $[Pd(Ph_3P)_2X]^-$ complexes. The effect of the linker was demonstrated to be associated with the capability or lack thereof of the neutral $Ph_2P(CH_2)_nPh_2P)Pd$ fragment to relax its geometry. Thus, dicoordinate Pd^0 complexes prefer a linear P-Pd-P structure (Figure 6a), and this geometric relaxation lowers the energy of the dicoordinate fragment complex. A short linker prevents this relaxation and thereby raises the bond dissociation energy.

In summary: theory shows that the postulated anionic active zero-valent palladium species in the Heck and cross-coupling reactions are true minima, albeit the bond energies between palladium and the anionic ligand are not very strong. The calculated geometric features and spectral properties will be helpful for eventual characterization of these complexes. A possible origin of their impact on the catalytic cycle can be deduced already from Figure 6. This has to do with the bent P-Pd-P angle that is promoted by the attachment of the additive, and can be rationalized using the valence bond diagrammatic model of chemical reactivity.[23] However, this will have to be proven yet by a complete calculation of the catalytic cycle.

Acknowledgement

The work was supported by a joint grant (from the Ministry of Sciences, Humanities and Sports to S.S. and from AFIRST to A.J. and C.A.).

[1] For a small selection of experimental papers, see: a) R. R. Tykwinski, *Angew. Chem.* **2003**, *115*, 1604–1606 ; *Angew. Chem. Int. Ed.* **2003**, *42*, 1566–1568; b) H. von Schenck, B. Akerman, M. Svensson, *J. Am. Chem. Soc.* **2003**, *125*, 3503–3508; c) D. A. Culkin, J. F. Hartwig, *Acc. Chem. Res.* **2003**, *36*, 234–245; d) S. Bhattacharyya, T. J. R. Weakley, M. Chaudhury, *Inorg. Chem.* **1999**, *38*, 5453–5456; e) J. Hassan, M. Sevignon, Ch. Gozzi, E. Schulz, M. Lemaire, *Chem. Rev.* **2002**, *102*, 1359–1469; f) Y. M. Kim, S. Yu, *J. Am. Chem. Soc.* **2003**,

 © 2004 Wiley-VCH Verlag GmbH & Co. KGaA, Weinheim

125, 1696–1697; g) E. Negishi, *Acc. Chem. Res.* **1982**, *15*, 340–348; h) E. Negishi, *J. Am. Chem. Soc.* **1987**, *109*, 2393–2401; i) I. P. Beletskaya, A. V. Cheprakov, *Chem. Rev.* **2000**, *100*, 3009–3066; j) A. F. Littke, G. C. Fu, *Angew. Chem.* **2002**, *114*, 4350–4386 ; *Angew. Chem. Int. Ed.* **2002**, *41*, 4176–4211; k) B. Trost, D. L. van Vranken, *Chem. Rev.* **1996**, *96*, 395–422; l) V. V. Grushin, *Organometallics* **2000**, *19*, 1888–1900; m) W. Cabri, I. Candiani, S. DeBernardinis, F. Francalanci, S. Penco, *J. Org. Chem.* **1991**, *56*, 5796–5800; n) W. Cabri, I. Candiani, *Acc. Chem. Res.* **1995**, *28*, 2–7; o) J. M. Brown, N. A. Cooley, *Organometallics* **1990**, *9*, 353–359.

[2] C. Amatore, A. Jutand, M. J. Medeiros, L. Mottier, *J. Electroanal. Chem.* **1997**, *422*, 125–132.

[3] C. Amatore, M. Azzabi, A. Jutand, *J. Am. Chem. Soc.* **1991**, *113*, 8375–8384.

[4] C. Amatore, A. Jutand, A. Suarez, *J. Am. Chem. Soc.* **1993**, *115*, 9531–9541.

[5] C. Amatore, A. Jutand, *J. Organomet. Chem.* **1999**, *576*, 254–278.

[6] C. Amatore, A. Jutand, *Acc. Chem. Res.* **2000**, *33*, 314–321.

[7] C. Amatore, E. Carre, A. Jutand, M. A. M'Barki *Organometallics* **1995**, *14*, 1818–1826.

[8] C. Amatore, E. Carre, A. Jutand, M. A. M'Barki, G. Meyer, *Organometallics* **1995**, *14*, 5605–5614.

[9] C. Amatore, A. Jutand, A. Thuilliez, *Organometallics* **2001**, *20*, 3241–3249.

[10] C. Amatore, A. Jutand, J. L. Ricard, S. Kozuch, S. Shaik, unpublished results

[11] For computational work of organometallic species, including Pd, using DFT and other methods, see for example: a) S. Niu, M. B. Hall, *Chem. Rev.* **2000**, *100*, 353–405; b) A. Sundermann, O. Uzan, J. M. L. Martin, *Chem. Eur. J.* **2001**, *7*, 1703–1711; c) A. Dedieu, *Chem. Rev.* **2000**, *100*, 543–600; d) B. Goldfuss, U. Kazmaier, *Tetrahedron* **2000**, *56*, 6493–6496; e) B. F. Straub, *J. Am. Chem. Soc.* **2002**, *124*, 14195–11420; f) K. Albert, P. Gisdakis, N. Rösch, *Organometallics* **1998**, *17*, 1608–1616; g) G. Frenking, N. Fröhlich, *Chem. Rev.* **2000**, *100*, 717–774; h) N. Koga, K. Morokuma, *Chem. Rev.* **1991**, *91*, 823–842.

[12] P. J. Hay, W. R. Wadt, *J. Chem. Phys.* **1985**, *82*, 299.

[13] Jaguar 4.2, Schrödinger, Inc., Portland, OR, **1991–2000**.

[14] Gaussian 98 (Revision A.7), M. J. Frisch, G. W. Trucks, H. B. Schlegel, G. E. Scuseria, M. A. Robb, J. R. Cheeseman, V. G. Zakrzewski, J. A. Montgomery, Jr., R. E. Stratmann, J. C. Burant, S. Dapprich, J. M. Millam, A. D. Daniels, K. N. Kudin, M. C. Strain, O. Farkas, J. Tomasi, V. Barone, M. Cossi, R. Cammi, B. Mennucci, C. Pomelli, C. Adamo, S. Clifford, J. Ochterski, G. A. Petersson, P. Y. Ayala, Q. Cui, K. Morokuma, D. K. Malick, A. D. Rabuck, K. Raghavachari, J. B. Foresman, J. Cioslowski, J. V. Ortiz, B. B. Stefanov, G. Liu, A. Liashenko, P. Piskorz, I. Komaromi, R. Gomperts, R. L. Martin, D. J. Fox, T. Keith, M. A. Al-Laham, C. Y. Peng, A. Nanayakkara, C. Gonzalez, M. Challacombe, P. M. W. Gill, B. G. Johnson, W. Chen, M. W. Wong, J. L. Andres, M. Head-Gordon, E. S. Replogle, J. A. Pople, Gaussian, Inc., Pittsburgh, PA, **1998**.

[15] a) A. Bergner, M. Dolg, W. Kuechle, H. Stoll, H. Preuss, *Mol. Phys.* **1993**, *80*, 1431; b) P. Fuentealba, L. V. Szentpaly, H. Preuss, H. Stoll, *J. Phys. B* **1985**, *18*, 1287; c) G. Igel-Mann, H. Stoll, H. Preuss, *Mol. Phys.* **1988**, *65*, 1321;

[16] a) Basis sets taken from http://www.emsl.pnl.gov/forms/basisform.html; b) J. M. L. Martin, A. Sundermann, *J. Chem. Phys.* **2001**, *114*, 3408; c) A. Bergner, M. Dolg, W. Kuechle, H. Stoll, H. Preuss, *Mol. Phys.* **1993**, *80*, 1431; d) D. E. Woon and T. H. Dunning, Jr. *J. Chem. Phys.* **1993**, *98*, 1358; e) A. K. Wilson, D. E. Woon, K. A. Peterson, T. H. Dunning Jr. , *J. Chem. Phys.* **1999**, *110*, 7667.

[17] a) D. J. Tannor, B. Marten, R. Murphy, R. A. Friesner, D. Sitkoff, A. Nicholls, M. Ringnalda, W. A. Goddard III, B. Honig, *J. Am. Chem. Soc.* **1994**, *116*, 11875–11882; b) B. Marten, K. Kim, C. Cortis, R. A. Friesner, R. B. Murphy, M. N. Ringnalda, D. Sitkoff, B. Honig, *J. Phys. Chem.* **1996**, *100*, 11775.

[18] a) Y. Ruiz Morales, T, Ziegler, *J. Phys. Chem. A* **1998**, *102*, 3970–3976; b) V. Robert, S. Petit, S. A. Borshch, B. Bigot, *J. Phys. Chem. A* **2000**, *104*, 4586–4591.

[19] The anionic complex $[Pd^0(PPh_3)_2Cl]^-$ was generated by the electrochemical reduction of $[Pd(PPh_3)_2Cl_2]$ (2 mM) in THF containing nBu$_4$NBF$_4$ (0.2 M) as the supporting electrolyte. It was characterized by a ^{31}P NMR singlet at 25.22 ppm versus H_3PO_4.[3] However, it is worthwhile to note that the chemical shift of this anionic species associated to the counter cation nBu$_4$N$^+$ must be sensitive to the ionic strength imposed by the supporting electrolyte. The experimental chemical shift of $[Pd^0(PPh_3)_2Cl]^-$ may also depend on the presence of cations that can interact with the chloride of the anionic species. This happens when $[Pd(PPh_3)_2Cl_2]$ is reduced by a chemical organometallic reductant. See: E. I. Negishi, T. Takahashi, K. Akiyoshi, *J. Chem. Soc. Chem. Commun.* **1986**, *1338*.

[20] R. Hoffmann, *Science* **1981**, *211*, 995–1002.

[21] T. A. Albright, J. K. Burdett, M. H. Whangbo, *Orbital Interactions in Chemistry*, Wiley-Interscience, **1985**

[22] A. D. Walsh, *J. Chem. Soc.* **1953**, 2288.

[23] S. Shaik, A. Shurki, *Angew. Chem.* **1999**, *111*, 616–657; *Angew. Chem. Int. Ed.* **1999**, *38*, 586–625; .

Received: December 22, 2003

Published online: April 29, 2004

 © 2004 Wiley-VCH Verlag GmbH & Co. KGaA, Weinheim